

Heat and Mass Transport From Thermally Degrading Thin Cellulosic Materials in a Microgravity Environment¹

G. Kushida²

H. R. Baum

T. Kashiwagi

Center for Fire Research,
National Institute of Standards and
Technology,
Gaithersburg, MD 20899

C. di Blasi

Chemical Engineering Department,
University of Naples,
Naples, Italy

A theoretical model describing the behavior of a thermally thin cellulosic sheet heated by external thermal radiation in a quiescent microgravity environment is developed. This model describes thermal and oxidative degradation of the sheet and the heat and mass transfer of evolved degradation products from the heated cellulosic surface into the gas phase. At present, gas phase oxidation reactions are not included. Without buoyancy, the dominant vorticity creation mechanism in the bulk of the gas is absent except at the material surface by the requirement of the no-slip condition. The no-slip condition is relaxed, permitting the flow to be represented by a velocity potential. This approximation is permissible due to the combination of a microgravity environment and low Reynolds number associated with slow small-area heating by external radiation. Two calculations are carried out: heating without thermal degradation, and heating with thermal degradation of the sheet with endothermic pyrolysis, exothermic thermal oxidative degradation, and highly exothermic char oxidation. The results show that pyrolysis is the main degradation reaction. Moreover, self-sustained propagation of smoldering for cellulosic materials is very difficult due to the lack of sufficient oxygen supply in a quiescent environment.

Introduction

Ignition of solid fuels by external thermal radiation is a process that not only is of considerable scientific interest but that also has fire safety applications. This process is complicated by strong coupling between chemical reactions and transport processes not only in the gas phase but also in the condensed phase. Although the fundamental processes involved in radiative auto-ignition have been suggested by Akita (1978), Kashiwagi (1979, 1981), and Mutoh et al. (1978), there have been no definitive experimental or modeling studies due to the flow motion generated by buoyancy near the heated sample surface. It is extremely difficult to solve theoretical models accurately. One must solve the full Navier–Stokes equations over an extended region to represent accurately the highly unstable buoyant plume. In order to avoid the complicated nature of the starting plume problem under normal gravity, previous detailed radiative ignition models were assumed to be one-dimensional (Kashiwagi, 1974; Kindelan and Williams, 1977) or were applied at the stagnation point (Amos and Fernandez-Pello, 1988). The mismatch between experimental and calculated geometries means that theories cannot be compared directly with experimental results in normal gravity.

To overcome the above difficulty, a theoretical and experimental study for ignition and subsequent transition of flame spread in microgravity has been supported by NASA's Microgravity Science Program. The objective of this study is to be able to compare the theoretical results quantitatively to the experimental data and to obtain a more definitive understanding of the ignition mechanism by the use of a microgravity environment. In this paper the description of the theoretical model and the calculated results of heat and mass transport near the heated surface during a preheating period are described. The model has been developed by taking advantage

of the microgravity environment as much as possible in the gas phase instead of modifying a conventional normal-gravity approach. Further extension including gas phase oxidation reactions to achieve ignition will be described in a future paper.

The theoretical model has been developed to be comparable to planned experiments in microgravity using NASA's two drop towers or the space shuttle. A thermally thin cellulosic sheet is considered as the sample fuel. Such a sample might ignite during test times available in the drop towers without requiring a pilot. This eliminates many complicating parameters such as pilot location, temperature, and size (Tzeng et al., 1990). The generation of high-temperature char at the sample surface acts as a self-induced pilot provided by highly exothermic char oxidation (Kashiwagi, 1981). The absorption of the external radiation by evolved degradation products in the gas phase (Amos and Fernandez-Pello, 1988; Kashiwagi, 1981) is not included in the model because a specific lamp, which emits the majority of its energy in near infrared, will be used to reduce the absorption as much as possible in the planned experiment. Although a slow flow along the sample surface, similar to a ventilation flow in a space craft, can have significant effects on the flame spread velocity (Olson et al., 1988), a quiescent environment is used first to develop the model.

2 Theory

2.1 Gas Phase Mathematical Model. The study of radiative ignition of solid fuels in a microgravity environment requires a description of time-dependent coupled processes in both the gas and condensed phases. The mathematical and computational complexity inherent in such a study suggests that the simplifications permitted by the microgravity environment and the small physical scale of the idealized experiment be built into the mathematical model. These simplifications principally affect the gas phase processes. The absence of gravity removes the buoyancy-induced vorticity generation mechanism. The small scale of the experiment, to-

¹Contribution from the National Institute of Standards and Technology.

²Guest researcher from Nagoya University, Nagoya, Japan.

Contributed by the Heat Transfer Division and presented at the ASME/JSME Thermal Engineering Conference, Reno, Nevada, March 17–22, 1991. Manuscript received January 1991; revision received October 1991. Keywords: Mass Transfer, Microgravity Heat Transfer, Transient and Unsteady Heat Transfer.

gether with the absence of any significant externally imposed velocity, implies a low Reynolds number flow domain (characteristic length is about 1 cm, which is half the width of an external thermal radiation beam in this study). Classical analyses of low Reynolds number flows have demonstrated that using the Oseen approximation to the convective terms in the equations of motion "constitutes an ad-hoc uniformization" (Van Dyck, 1964) of the first approximation to the rigorous calculation of the flow past isolated bodies. The central point that emerges from these analyses is that diffusion dominates convection near the surface, so the fact that the Oseen flow does not satisfy the no-slip boundary condition is irrelevant at the lowest order in the theory. When surface pyrolysis or evaporation is present, the thermally induced surface blowing velocity must be taken into account, even at low Reynolds numbers. Both these concepts can be accommodated by assuming the velocity field to a potential flow. The uniform Oseen velocity is of course a trivial potential flow. The generalization to a flow past an arbitrarily shaped body with a prescribed surface blowing distribution can also be accommodated by a potential field, if vorticity generated in the interior of the flow can be ignored. Again, the only loss is the no-slip boundary condition. This approximation is adopted and is implicit in the analysis that follows.

The potential flow description of the velocity field greatly simplifies both the formulation and subsequent computation of a wide variety of low Reynolds number microgravity heat transfer and combustion problems. Accordingly, the formulation will be developed in a fairly general context and then specialized to the specific case of the radiative ignition of a thermally thin fuel. The starting point is the conservation of mass and energy in the gas. Under low Mach number combustion/heat transfer conditions, these equations can be written as:

$$D\rho/Dt + \rho \nabla \cdot \mathbf{v} = 0$$

$$\rho C_p DT/Dt - \mathbf{v} \cdot (k \nabla T) = \dot{q}_R(\mathbf{r}, t) \quad (1)$$

Here, $\dot{q}_R(\mathbf{r}, t)$ is the net chemical and radiative heat release per unit volume into the gas of density ρ , temperature T , and velocity \mathbf{v} . The gas specific heat C_p and thermal conductivity k are in general functions of T . These equations are supplemented by an equation of state, taken in a form appropriate for low-Mach-number flows.

$$\rho h = \rho_\infty h_\infty$$

$$h = \int_0^T C_p(T) dT \quad (2)$$

The subscript ∞ refers to a suitable ambient or reference condition. This form allows C_p to vary with temperature without doing too much violence to the equation of state over

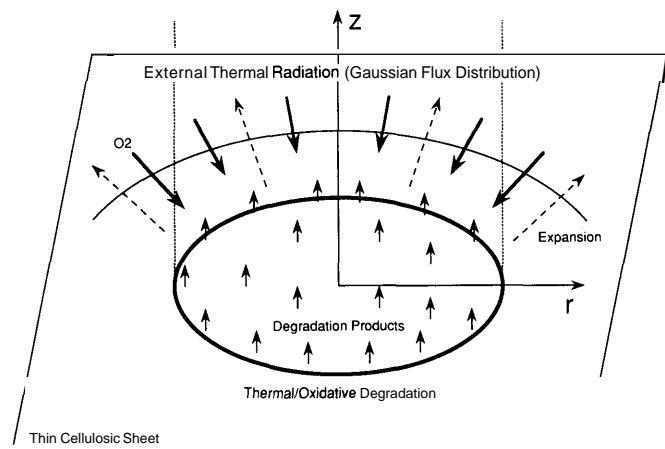


Fig. 1 Schematic radiative ignition process

temperature ranges appropriate to hydrocarbon combustion problems.

Now multiply the first of Eqs. (1) by h and add it to the second. The result, after using Eq. (2), is:

$$\rho_\infty h_\infty \nabla \cdot \mathbf{v} - \nabla \cdot (k \nabla T) = \dot{q}_R(\mathbf{r}, t) \quad (3)$$

Equation (3) is the fundamental equation for determining the velocity field \mathbf{v} . Since \mathbf{v} is a vector field, it can be decomposed into the gradient of a potential ϕ and a solenoidal field \mathbf{u} .

$$\mathbf{v} = \nabla \phi + \mathbf{u}$$

$$\nabla \cdot \mathbf{u} = 0 \quad (4)$$

Substitution of Eq. (4) into Eq. (3) yields:

$$\nabla^2 \phi = (1/\rho_\infty h_\infty) (\dot{q}_R(\mathbf{r}, t) + \nabla^2 \psi)$$

$$\psi = \int_{\mathbf{r}_\infty}^T k(T) dT \quad (5)$$

Note that the second term on the right-hand side of Eq. (5) can be eliminated by introducing a particular solution ϕ_p as:

$$\phi_p = \psi / \rho_\infty h_\infty \quad (6)$$

Then, introducing a remainder potential $\Phi(\mathbf{r}, t)$, ϕ may be expressed in the form:

$$\phi = \phi_p + \Phi(\mathbf{r}, t)$$

$$\nabla^2 \Phi = \dot{q}_R(\mathbf{r}, t) / h_\infty \rho_\infty \quad (7)$$

Equations (6) and (7) relate the potential field to the temperature and species distributions in the gas phase. Since it is necessary to determine these latter quantities in any event,

Nomenclature

A = pre-exponential frequency factor
 C, C_p = specific heat
 D = mass diffusivity
 E = activation energy
 H = heat of reaction
 h = enthalpy
 K = complete elliptic integral of the first kind
 k = thermal conductivity
 m = mass flux of gas through condensed phase surface
 Q = heat flux
 \dot{q}_R = net chemical and radiative heat release
 R = universal gas constant

RR = reaction rate of solid species
 T = temperature
 t = time
 r = radial coordinate
 \mathbf{u}, \mathbf{v} = velocity vectors
 Y = mass fraction
 z = axial coordinate
 δ = thickness of paper
 ϵ = emissivity
 ν = stoichiometric coefficient
 ρ = density
 σ = Stefan-Boltzmann constant
 Φ, ϕ = potential function

Subscripts

C = char

F = fuel
 G = gas
 OX = oxygen
 rad = radiation
 S = solid
 $0, \infty$ = ambient or reference condition
 1 = associated with reaction 1 (pyrolysis)
 2 = associated with reaction 2 (thermal oxidative degradation)
 3 = associated with reaction 3 (char oxidation)

solution of Eq. (7) represents the minimum additional work required to obtain a self-consistent velocity field. Implied in this statement is the assumption that the solenoidal velocity field \mathbf{u} is not of interest in its own right. If \mathbf{u} is of interest, then there is no alternative to solving the Navier-Stokes equations. However, a large portion of both the combustion and heat transfer literature consists of calculations in which the details of the velocity field are approximated, often crudely, in order to understand the thermophysical phenomenon of direct interest. In the present circumstances, the approximations have been justified in simple geometries by detailed analyses, and interest will be confined to species and temperature fields induced by radiative ignition.

Now consider the specific problem of a concentrated radiation source impinging on a thermally thin fuel slab. The geometry is shown in Fig. 1. Let r and z be radial and axial cylindrical coordinates as shown in the figure. Attention is focused on the preheating phase of the ignition process. The gas is assumed to be transparent to the radiation. Under these circumstances, the term $\dot{q}_R(\mathbf{r}, z, t)$ in Eqs. (1) can be ignored. The gas phase energy and species conservation equations take the form:

$$\rho C_p (\partial T / \partial t + \nabla \phi \cdot \nabla T) = \nabla \cdot (k \nabla T)$$

$$\rho (\partial Y_i / \partial t + \nabla \phi \cdot \nabla Y_i) = \nabla \cdot (\rho D \nabla Y_i) \quad (8)$$

Here, Y_i are the mass fractions of the oxygen Y_{O_2} , and the fuel species Y_F emitted by the pyrolyzing solid located at $z=0$. The diffusivity D , thermal conductivity k , specific heat C_p , and density ρ are assumed to be independent of the gas species but dependent on temperature. The values for air are used to represent these properties and the polynomial fitting of temperature for each property is used in the calculation. These equations are to be solved together with Eqs. (6) and (7), subject to boundary and initial conditions.

At time $t=0$, the entire system is assumed to be at rest at (cool) ambient temperature T_∞ . Hence:

$$\phi(\mathbf{r}, z, 0) = Y_F(\mathbf{r}, z, 0) = 0$$

$$Y_{O_2}(\mathbf{r}, z, 0) = Y_\infty$$

$$T(\mathbf{r}, z, 0) = T_\infty \quad (9)$$

Once the heating process has started, the solid fuel temperature $T_S(\mathbf{r}, t)$ rises above ambient and at some later time a mass flux $\dot{m}(\mathbf{r}, t)$ of gasified fuel is evolved from the fuel surface. The gas phase boundary conditions can be expressed in terms of these quantities as:

$$\partial \phi(\mathbf{r}, 0, t) / \partial z = h(\mathbf{r}, 0, t) \dot{m}(\mathbf{r}, t) / \rho_\infty h_\infty$$

$$h(\mathbf{r}, 0, t) = \int_0^{T_S} C_p dT$$

$$T(\mathbf{r}, 0, t) = T_S(\mathbf{r}, t)$$

$$\dot{m}(\mathbf{r}, t) = \rho_\infty h_\infty \{ \partial \phi(\mathbf{r}, 0, t) / \partial z \} Y_F(\mathbf{r}, 0, t) / h(\mathbf{r}, 0, t)$$

$$- \rho_\infty h_\infty D(\mathbf{r}, 0, t) \{ \partial Y_F(\mathbf{r}, 0, t) / \partial z \} / h(\mathbf{r}, 0, t) \quad (10)$$

Alternatively, the residual potential Φ is subject to the boundary condition:

$$\partial \Phi(\mathbf{r}, 0, t) / \partial z = \{ h(\mathbf{r}, 0, t) \dot{m} - k \partial T(\mathbf{r}, 0, t) / \partial z \} / \rho_\infty h_\infty \quad (11)$$

Equation (11) replaces the first of Eqs. (10).

Far from the surface, ϕ , Y_i , and T must decay to their ambient initial values. Translating this into boundary conditions suitable for numerical computation, however, requires some care. Numerical boundary conditions are applied at the edge of a rectangular computational domain. Since Y_i and T decay exponentially to their ambient values, setting these quantities equal their values given in Eq. (9) is permissible until the first calculated nonambient contours of these quantities approach the computational boundary. However, the potential field decays slowly away from the heated region, i.e.,

Table 1 Chemical properties of thermal degradation

	A	E [kJ/mol]	ν_C	ν_G	ν_{O_2}	ν_A	ΔH [J/g]
(1)	1.4×10^{19} [min ⁻¹]	220	0.27	0.73			+570
(2)	1.0×10^{17} [cm ³ /g min]	170	0.27	0.83	0.10		-4.200
(3)	1.0×10^{13} [cm ³ /g min]	160		2.00	1.00	0.00	-25,000

$\phi \sim (r^2 + z^2)^{-1}$. Thus, putting ϕ or its gradient equal to zero at the computational boundary would introduce unacceptable errors into the calculation. These errors can be avoided by using the solution to Eq. (7) (with $\dot{q}_R=0$) subject to the boundary condition given by Eq. (11).

$$\rho_\infty h_\infty \Phi = \int_0^\infty G(\mathbf{r}, r_0, z) \partial \Phi(r_0, 0, t) / \partial z r_0 dr_0$$

$$G(\mathbf{r}, r_0, z) = (2/\pi) K(k_b) / [(r+r_0)^2 + z^2]^{1/2}$$

$$k_b^2 = 4rr_0 / [(r+r_0)^2 + z^2] \quad (12)$$

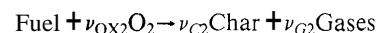
Here K is the complete elliptic integral of the first kind. Now $\partial \Phi(r_0, 0, t) / \partial z$ is given by Eq. (11) at any instant of time, and the temperature is an exponentially decaying function of the radial integration variable in Eq. (12). Hence, use of Eq. (12) to evaluate Φ around the computational boundary provides a fast and highly accurate means of applying computational boundary conditions to Φ .

2.2 Condensed Phase Mathematical Model. In the present paper the condensed phase is initially a cellulosic sheet that changes gradually to char followed by ash, due to thermal degradation. The phase is assumed to be thermally thin and also depth-wise uniform in its composition. Although there are numerous studies on the thermal degradation of cellulose and wood (for example, Nakagawa and Shafizadeh, 1984), the expression of mass addition rates from a thermally degrading paper in air is needed in this study. Since detailed study of oxidation reactions of a paper and char is limited, a global approach of three reactions (Rogers and Ohlemiller, 1980) is used in this study.

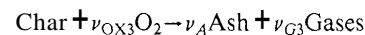
(1) Endothermic Pyrolysis Reaction. The cellulosic material is endothermically degraded to a char.



(2) Exothermic Thermal Oxidative Degradation Reaction. The cellulosic material is exothermically degraded to a char by oxidation. Generally, this reaction occurs in approximately the same temperature range as for the pyrolysis reaction.



(3) Exothermic Char Oxidation Process. The char formed by the above reactions is exothermically reacted with oxygen to form gases and ash. Here, it is assumed that the reactivity of char formed from the above two reactions with oxygen is the same.



In the above three reactions, the reaction rates RR , are assumed to be given by the following expressions:

$$(1) RR_1 = A_1 (\rho_S Y_F) \exp(-E_1/RT)$$

$$(2) RR_2 = A_2 (\rho_G Y_{O_2}) (\rho_S Y_F) \exp(-E_2/RT)$$

$$(3) RR_3 = A_3 (\rho_G Y_{O_2}) (\rho_S Y_C) \exp(-E_3/RT) \quad (13)$$

Here, the pre-exponential frequency factor A , activation energy E for each reaction, stoichiometric coefficients (mass based) of species ν_C , ν_G , ν_{O_2} , and ν_A must be specified. Although these reactions are assumed to be first order and second

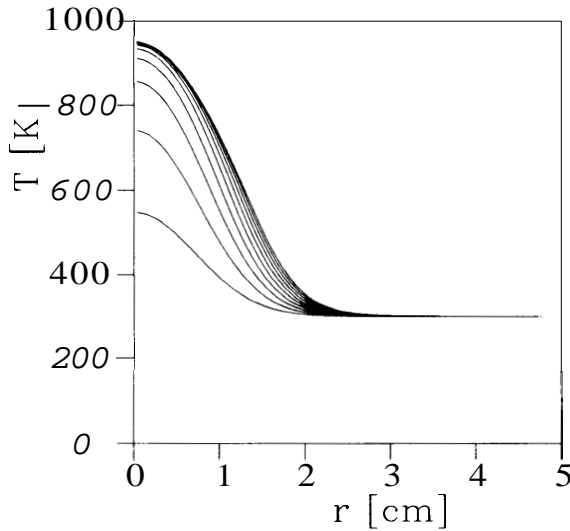


Fig. 2 Radial distribution of material surface temperature, at 1 s intervals

order, any other order of reaction can be used in the model. These parameters together with the heats of reaction ΔH are given in Table 1. The values for the pyrolysis reaction are measured by conducting a thermogravimetric analysis of a black paper that has been used for preliminary ignition experiments under normal gravity. The results of derivative thermogravimetry are analyzed by Kissinger's method (Kissinger, 1957). Although the measurement of kinetic constants for the above two oxidative reactions is in progress, the values listed for the two oxidative degradations are estimated from our preliminary results. A parametric study regarding values of kinetic constants for the two oxidative reactions has been conducted and the results are described in the final portion of this paper.

The equations for the condensed phase are given as follows:

Conservation of solid mass:

$$\partial \rho_S / \partial t = (\nu_{C1} - 1)RR_1 + (\nu_{C2} - 1)RR_2 + (\nu_A - 1)RR_3 \quad (14)$$

Conservation of cellulosic material:

$$\partial (\rho_S Y_F) / \partial t = -RR_1 - RR_2 \quad (15)$$

Conservation of char:

$$\partial (\rho_S Y_C) / \partial t = \nu_{C1}RR_1 + \nu_{C2}RR_2 - RR_3 \quad (16)$$

Conservation of energy:

$$(C_F \rho_S \delta) \partial T_s / \partial t = (-\Delta H_1 RR_1 - \Delta H_2 RR_2 - \Delta H_3 RR_3) \delta + (1-r)Q_{rad} - \epsilon \sigma (T_s^4 - T_\delta^4) + k \partial T / \partial z + \dot{m} (h_s - h(r, \theta, t)) \quad (17)$$

where δ is the thickness of the paper and the heat flux distribution of the external radiation is assumed to be Gaussian. In the calculation reported here,

$$Q_{rad} = 50 \exp(-\alpha r^2) \quad [\text{kW/m}^2] \quad (18)$$

where $\alpha = 1.0 \times 10^4 \text{ [m}^{-2}\text{]}$. The reflectivity, r , is assumed to be 0 and the emissivity, ϵ , is assumed to be 1.

The mass flux of gasified fuel through the sample surface is given by the following expression:

$$\dot{m} = [(1 - \nu_{C1}RR_1 + (1 - \nu_{C2})RR_2 + (1 - \nu_A)RR_3) \times \delta] \quad (19)$$

The cellulosic material used in the present study is a $0.25 \times 10^3 \text{ m}$ thick paper sheet. The properties are: $C_S (=C_F=C_C) = 1.255 \text{ [kJ/(kgK)]}$, $k_S = 6.0 \times 10^{-2} \rho_S / \rho_F \text{ [W/(mK)]}$ (Nakagawa and Shafizadeh, 1984), $\rho_F = 0.6 \times 10^{-3} \text{ [kg/m}^3\text{]}$.

2.3 Numerical Methods. The numerical calculation is performed by using a finite-difference method. The compu-

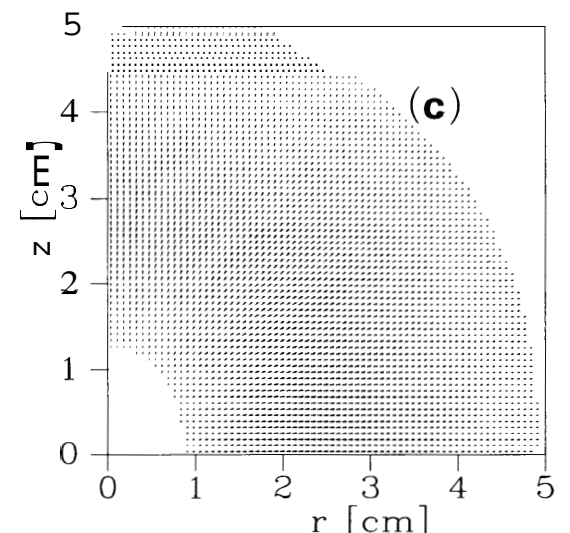
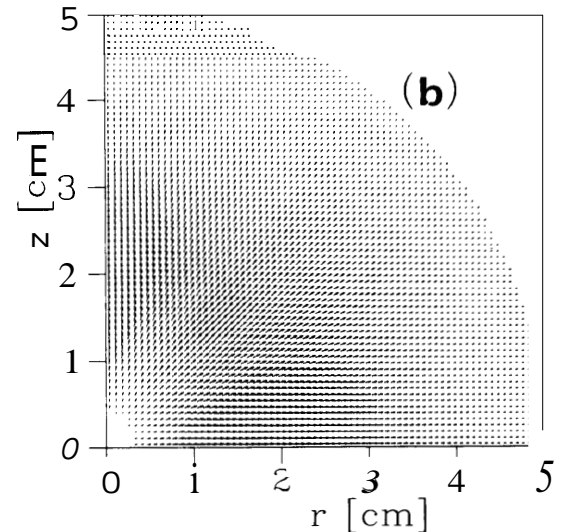
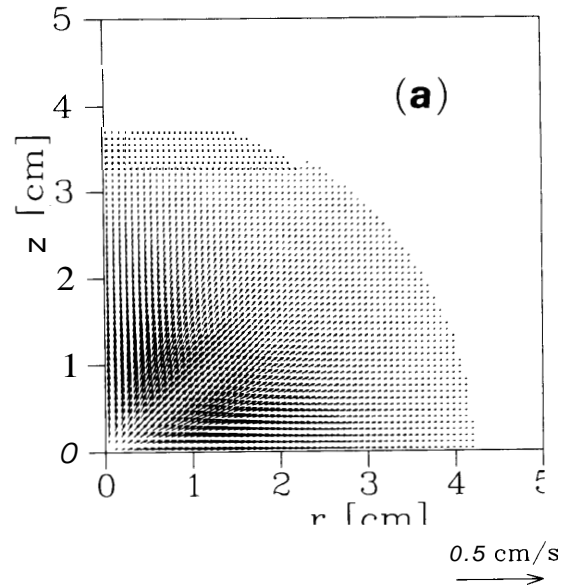


Fig. 3 Velocity vector distributions at (a) 1 s, (b) 3 s, and (c) 5 s (velocity vectors less than 1/40 of 0.5 cm/s are not plotted in the figure)

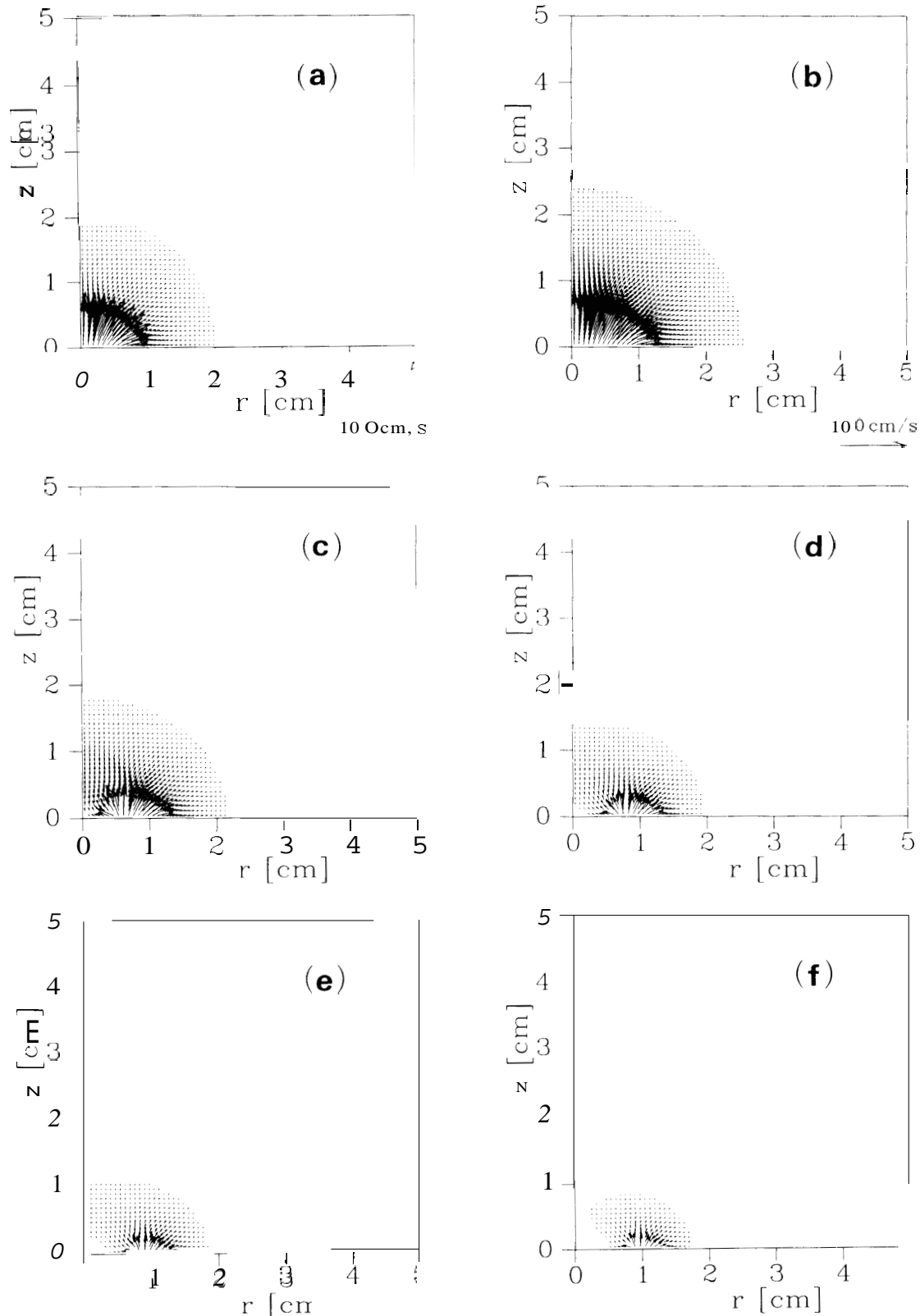


Fig. 4 Velocity vector distribution at (a) 2.0 s, (b) 3.5 s, (c) 5 s, (d) 6.5 s, (e) 8.0 s, (f) 9.5 s (velocity vectors less than 1/40 of 100 cm/s are not plotted in the figure)

tational domain is taken to be $r \leq 5.0$ cm and $z \leq 5.0$ cm. There are 71 and 72 grid cells in the r and z directions, respectively. The grid size was chosen after numerical experiments at half size together with Richardson extrapolation showed that the error is within 0.4 percent.

The equations to be solved for the gas phase are those for the potential function Φ , the temperature T , and the species Y_{Ox} . For the condensed phase, the equations for the temperature T , the species Y_F and Y_C , and the solid density ρ_S also have to be solved. Since the condensed phase temperature

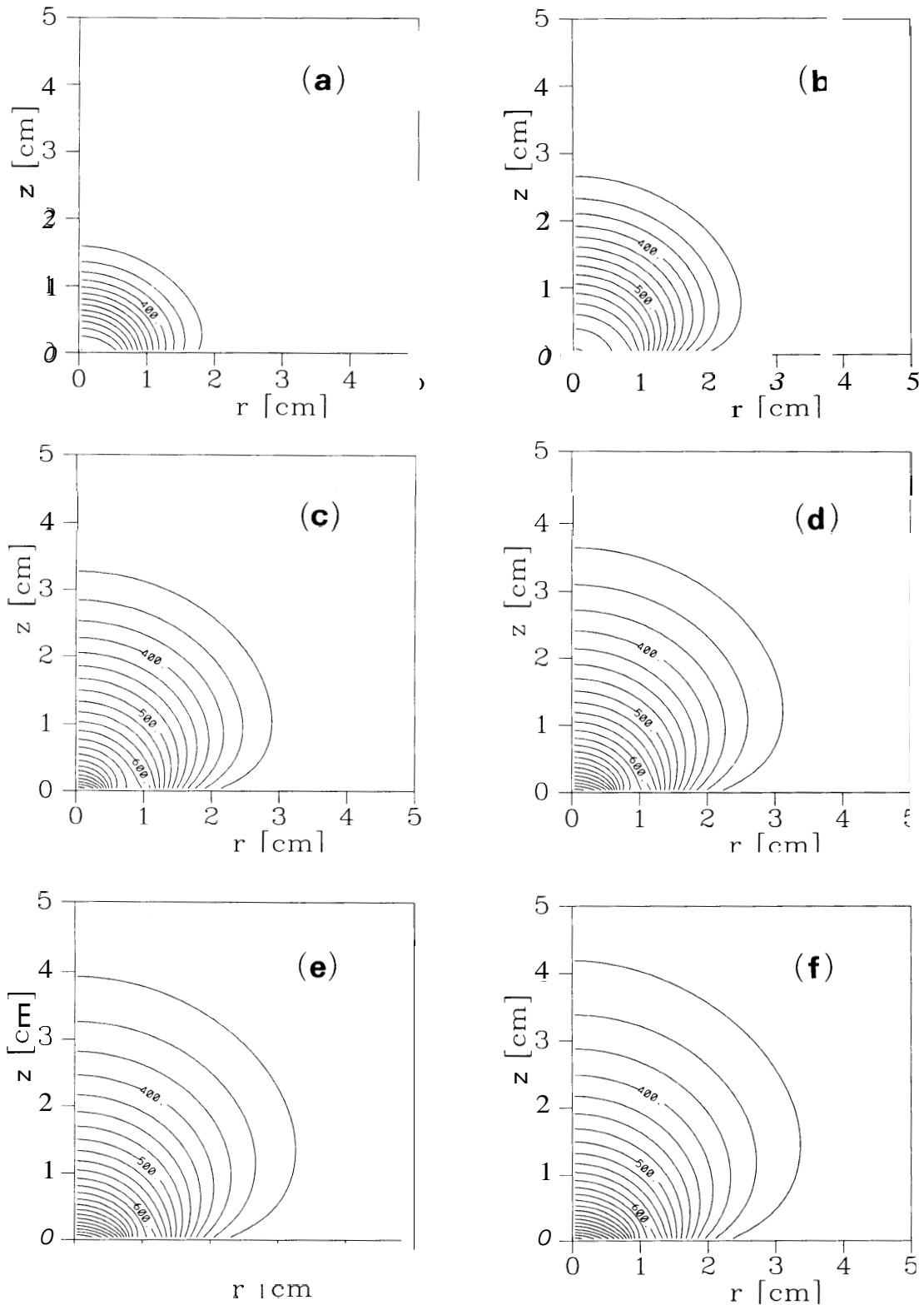


Fig. 5 Gas phase temperature contours at (a) 2.0 s, (b) 3.5 s, (c) 5.0 s, (d) 6.5 s, (e) 8.0 s, and (f) 9.5 s, at intervals of 25 K

equation is coupled with that for the gas phase, the two equations are solved simultaneously in the present analysis. The solution for Φ is computed by employing a direct solver of the Poisson equation in cylindrical coordinates using the standard five-point finite difference approximation on a staggered grid (FISHPAK). The equations for temperature and gas species employ a second-order difference scheme for both convection

and diffusion terms. The boundary conditions for Φ are specified at the open boundaries by calculating Eq. (12). The derivative of the solution with respect to z is specified at $z=0$ by Eq. (11). As for the boundary conditions for temperature and species for the gas phase, the derivatives are taken to be zero at the open boundaries. The derivative of species with respect to z is also taken to be zero at $z=0$.

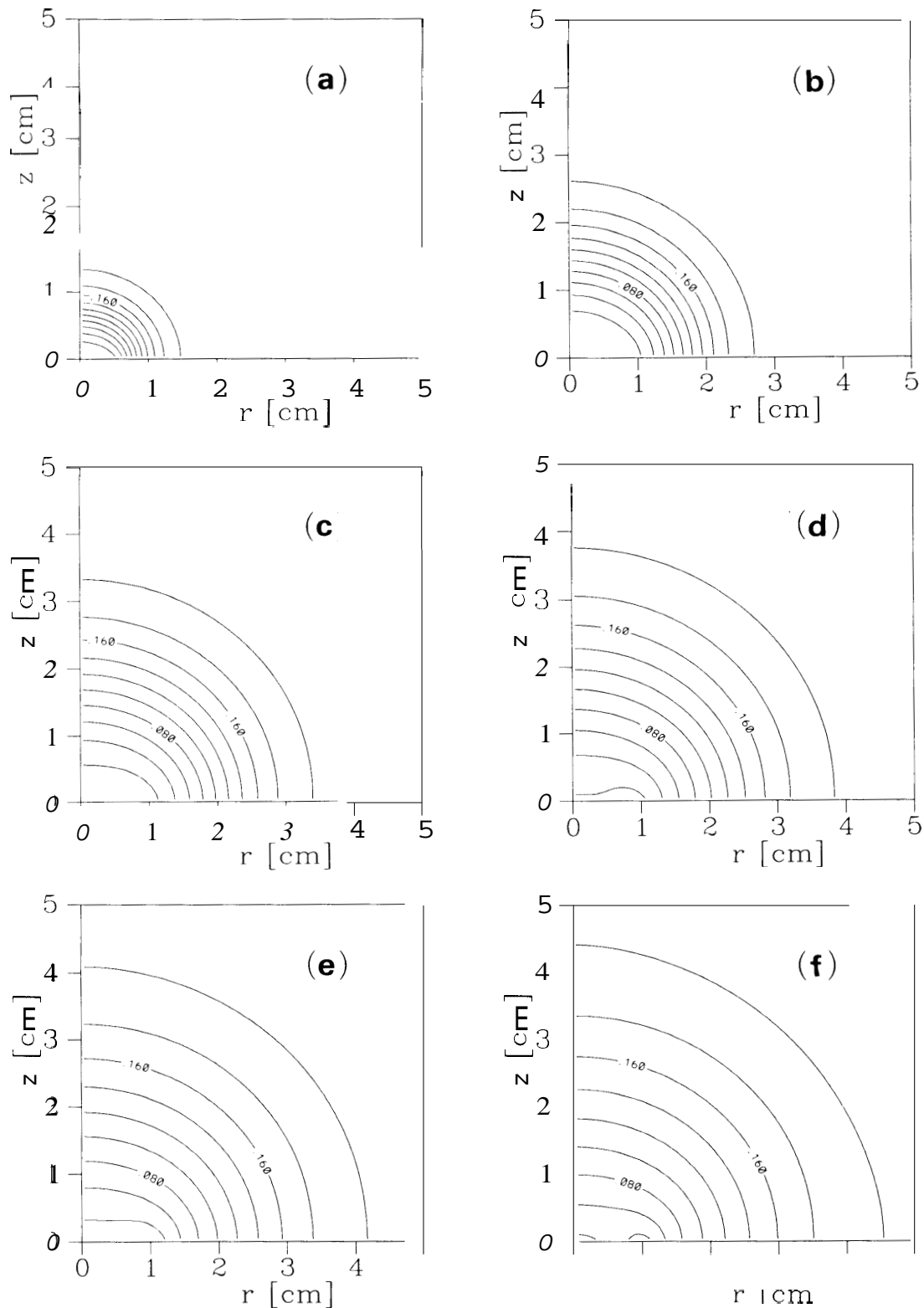


Fig. 6 Gas phase oxygen contour at (a) 2.0 s, (b) 3.5 s, (c) 5.0 s, (d) 6.5 s, (e) 8.0 s, and (f) 9.5 s at intervals of 0.02

The temperature variation with respect to the z direction in the condensed phase is ignored, because it is assumed to be thermally thin. The oxidation of the condensed phase is performed by consuming the oxygen in the control volume immediately above the sample surface. It is also assumed that the condensed phase does not become porous. Only the density

of the solid material changes. The other equations ((14)–(17)) for the condensed phase are also solved using a finite difference approximation for a control volume of the same size as that in the gas phase. The time advance is made by using Euler's implicit method with an interval of 0.025 seconds, which satisfies the error estimate stated above.

3 Results and Discussion

3.1 Results Without Thermal Degradation. Figure 2 shows the change in the radial temperature distribution of the sample with time without the thermal degradation of the solid material. The temperature distribution corresponds to the Gaussian flux distribution of external radiation expressed by Eq. (18). The temperature increase slows down significantly at about 7 seconds because of the heat balance between external radiation and the reradiation loss from the high-temperature surface.

Figures 3 show the velocity vector distributions at 1, 3, and 5 seconds after irradiation, respectively. As shown in the figures, the gas phase is heated by heat conduction from the sample surface irradiated by external radiation, and the region of heated gas expands as time increases. The gas flow changes from the initial quiescent state into the outward flow motion from the region near the heated surface due to the expansion of the gas. The flow velocity gradually decreases after about 5 seconds and becomes almost zero everywhere in 10 seconds, although irradiation of the surface by the external radiation is still continued. In the absence of thermal degradation, the magnitude of the velocity is small for all times.

3.2 Results With Thermal Degradation. The results including the thermal degradation of the cellulosic sheet described in section 2.2 are shown in Figs. 4, 5, and 6, giving velocity vector distributions, temperature contours, and oxygen concentration contours up to 9.5 seconds, respectively. These show a rapid increase in flow velocity near the sample surface due to mass addition after the sample temperature becomes sufficiently high to cause thermal degradation. Blowing starts to become significant at about 1.5 seconds and continues to increase until about 3.5 seconds. Flow velocities normal to the sample surface with thermal degradation become as large as 50 times those without thermal degradation (shown in Fig. 3). Therefore, blowing significantly affects the flow motion in microgravity. (It should be noted, however, that local Reynolds numbers based on the velocity and distance from the axis of symmetry are still $O(1)$.) Correspondingly, the high gas temperature region is expanded much further by the blowing due to thermal degradation. The mass addition of degradation gases rapidly dilutes the oxygen concentration near the heated sample surface. At about 2 seconds, the oxygen concentration at the center of the sample near the sample surface is nearly zero. This indicates that thermal degradation is mainly due to the pyrolysis reaction instead of the oxidative degradation reactions. After 4 seconds the location of maximum blowing velocity gradually moves from the center radially outward because the original cellulosic material is nearly consumed as the hard-to-degrade char is formed. In this way, the char region gradually expands from the center outward and the blowing nearly stops over the char region. The temperature contours indicate that near the axis heat flows from the hotter surface to the cooler gas phase. In the region where blowing is active, convection by degradation products from the surface to the gas phase is dominant. In the region outside of the pyrolyzing zone, the gas phase temperature near the surface is higher than that of surface, giving temperature contours that have a different shape from the oxygen concentration contours; the latter are nearly normal to the surface, indicating that there is little consumption by the oxidative reactions.

Changes in the radial temperature distribution of the cellulosic sheet with time are shown in Fig. 7. Similarly the radial density distribution of the sheet is shown in Fig. 8. As seen on the axis in Fig. 7, the temperature rapidly rises in the first few seconds, but the increase slows after the temperature reaches about 650 K. This slowdown is caused by the endothermic pyrolysis reaction, which becomes significant in this temperature range. After the temperature remains at about

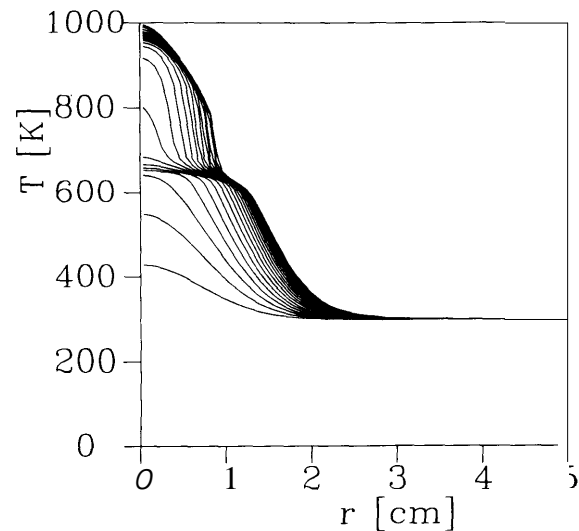


Fig. 7 Radial distribution of material temperature at intervals of 0.5 s

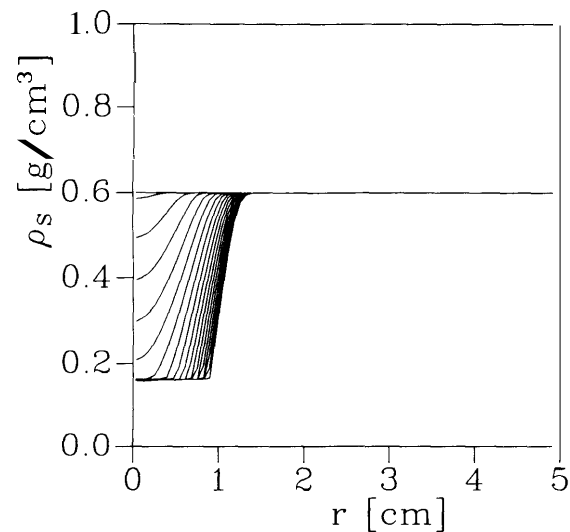


Fig. 8 Radial distribution of material density at intervals of 0.5 s

650 K for few seconds, it rapidly rises close to 1000 K and then slows again at about 4 seconds. This rapid temperature increase is caused by the complete consumption of the original cellulosic material to form char, which reduces the endothermic pyrolysis reaction rate and also the mass of the sample (the density of cellulose is roughly four times larger than that of char (Nakagawa and Shafizadeh, 1984)) and furthermore decreases blowing convective cooling from the hot surface. Energy is balanced at the sample surface mainly between the external radiation and the reradiation loss from the high-temperature surface.

The density of the material rapidly decreases from the initial value of 0.6 g/cm³ to about 0.16 g/cm³, which is the value of the char density. After about 4 seconds the density of the material remains at about 0.16 g/cm³, which indicates that the char oxidation reaction rate is not significant. The oxygen concentration contours show that oxygen concentration is extremely small at the sample surface in the region of active blowing, due mainly to dilution and poor oxygen supply by diffusion. Therefore, the oxidative degradation reaction and the char oxidative reaction do not participate significantly in the gasification process at an external radiant flux peak of 50 kW/m² in a quiescent environment. However, if there is a forced slow air flow along the sample surface such as a ventilation flow in a space craft, the oxidative degradation re-

actions might become important. Another possible scenario permitting char oxidation participation might occur if diffused oxygen leaks behind the outward moving blowing front generated by the pyrolysis reaction. A gradual increase in oxygen concentration near the axis by the sample surface can be observed from the oxygen concentration contours at 6.5 seconds. A slight dip in the contour of 2 percent oxygen concentration near the axis shows increased oxygen supply to this region by diffusion. This trend continues, and oxygen concentration reaches about 2.7 percent at 7 seconds. At this time the lowest oxygen concentration at the sample surface is in the region of active blowing at this time. However, this active blowing region gradually moves radially outward due to the consumption of the original cellulosic material. The level of blowing gradually decreases with increasing radius because the material temperature decreases with decrease in external flux. At 8 seconds the oxygen concentration near the axis reaches 3.5 percent. At 8.5 seconds the char oxidation reaction starts and the oxygen concentration near the surface decreases slightly. At 9 seconds within a 0.5 cm radius, the oxygen concentration near the surface decreases further due to the consumption of oxygen by the char oxidation reaction. The low oxygen concentration zone near the surface around 1 cm is due to dilution by degradation gases from the pyrolysis reaction. Since the temperature of the material is the highest at the axis, as shown in Fig. 7, due to Gaussian distribution of the external radiation, the char oxidation occurs only around the axis. However, the radial material density distribution, Fig. 8, indicates that a decrease in density by the consumption of char by oxidation is extremely small due to the lack of oxygen supply; the oxygen supply remains small due to dilution by degradation gases from the char oxidation reaction. Therefore, in a quiescent environment under microgravity the rate-controlling process for smoldering is the oxygen supply. The above results show that the two exothermic oxidative degradation reactions are severely limited even with continued external radiation. Therefore, self-supported smoldering (without external heat) of a cellulosic material is very difficult in a quiescent environment under microgravity.

3.3 Effect of Chemical Properties on Oxidation. These calculations were carried out using estimated values of the kinetic constants for the two oxidative degradations. Therefore, it might be premature to conclude that self-supported smoldering is severely limited in a quiescent environment under microgravity. A parametric study to examine effects of the kinetic constants for the two oxidation reactions on smoldering was conducted. Two types of calculations were performed; different kinetic constants for the oxidative degradation reactions were used in the above model, and a one-dimensional model ignoring gas phase phenomena was employed. The latter is basically a degradation kinetic model of the sheet with the specified initial oxygen concentration. Oxygen is consumed only by oxidation, and there is no oxygen supply or dilution by degradation gases. Although this model is limited to degradation of the sheet, the calculated results clearly show how the pyrolysis reaction and the two oxidative reactions compete to consume the cellulosic material and the oxygen. Since the calculation of the second model is much simpler, many cases were investigated using this model. The results indicate that smoldering tends to occur with lower values of ν_{OX2} and ν_{OX3} , higher values of ν_{C1} and ν_{C2} , and higher values of heat of oxidative degradations. The first reduces the consumption of oxygen, the second reduces the dilution by degradation gases, and the third increases energy heat release rates from the oxidative reactions. The effects of pre-exponential parameters

and activation energies do not significantly affect the trend of self-supported smoldering and they mainly change the temperature at which each degradation reaction occurs. Therefore, in order to predict smoldering characteristics of a cellulosic material in a microgravity environment, the values of kinetic constants for the above three global degradation reactions must be determined.

4 Conclusion

The following conclusions are derived from the calculated results in a *quiescent* environment under microgravity.

- 1 The flow motion created by heat addition from the surface to the gas phase rapidly dies out even when heat is continuously added.
- 2 The mass addition of degradation products from the surface to the gas phase generates relatively large flow velocities near the surface up to 10 cm/s at an external radiant flux of 50 kW/m² and surface absorptivity of 1 (compared with the nonblowing case) and dominates the motion.
- 3 The degradation gases are mainly generated from the pyrolysis degradation reaction. The oxidative degradation reaction is severely limited due to the lack of oxygen supply caused by dilution by the degradation gases emitted from the pyrolysis reaction at external radiation of 50 kW/m² and surface absorptivity of 1.
- 4 Char oxidation could occur near the axis of symmetry as oxygen gradually diffuses back to the char surface after the pyrolysis process is completed.
- 5 Self-sustained smoldering is controlled and severely limited by the reduced oxygen supply.

Acknowledgments

This study is supported by the NASA Microgravity Science Program under the Inter-Agency Agreement No. C-32000-K.

References

- Akita, K., 1978, "Ignition of Polymers and Flame Propagation on Polymer Surface," in: *Aspects of Degradation and Stabilization of Polymers*, H. H. G. Jellinek, ed., Elsevier Scientific, Chap. 10.
- Amos, B., and Fernandez-Pello, A. C., 1988, "Model of the Ignition and Flame Development on a Vaporizing Combustible Surface in a Stagnation Point Flow: Ignition by Vapor Fuel Radiation Absorption," *Combustion Science Technology*, Vol. 62, pp. 331-343.
- Kashiwagi, T., 1974, "A Radiative Ignition Model of a Solid Fuel," *Combustion Science Technology*, Vol. 8, pp. 225-236.
- Kashiwagi, T., 1979, "Experimental Observation of Radiative Ignition Mechanisms," *Combustion Flame*, Vol. 34, pp. 231-244.
- Kashiwagi, T., 1981, "Radiative Ignition Mechanism of Solid Fuels," *Fire Safety Journal*, Vol. 3, pp. 185-200.
- Kindelan, M., and Williams, F., 1977, "Gas-Phase Ignition of a Solid With In-Depth Absorption of Radiation," *Combustion Science Technology*, Vol. 16, pp. 47-58.
- Kissinger, H., 1957, "Reaction Kinetics in Differential Thermal Analysis," *Analytical Chem.*, Vol. 29, pp. 1702-1706.
- Mutoh, N., Hirano, T., and Akita, K., 1978, "Experimental Study on Radiative Ignition of Polymethylmethacrylate," *Seventeenth Symposium (International) on Combustion*, The Combustion Institute, Pittsburgh, PA, pp. 1183-1190.
- Nakagawa, S., and Shafizadeh, F., 1984, *Handbook of Physical and Mechanical Testing of Paper and Paperboard*, R. E. Mark, ed., Marcel Dekker, New York, Vol. 2, Chap. 23.
- Olson, S. L., Ferkul, P. V., and Tien, J. S., 1988, "Near-Limit Flame Spread Over a Thin Solid Fuel in Microgravity," *Twenty Second Symposium (International) on Combustion*, The Combustion Institute, Pittsburgh, PA, pp. 1213-1222.
- Rogers, F. E., and Ohlemiller, T. J., 1980, "Cellulosic Insulation Material I. Overall Degradation Kinetics and Reaction Heats," *Combustion and Science Technology*, Vol. 24, pp. 129-137.
- Tzeng, L. S., Atreya, A., and Wichman, I. S., 1990, "A One-Dimensional Model of Piloted Ignition," *Combustion and Flame*, Vol. 80, pp. 94-107.
- Van Dyck, M., 1964, *Perturbation Methods in Fluid Mechanics*, Academic Press, New York, pp. 149-158.

